Arch Appl Mech (2018) 88:1139–1161
https://doi.org/10.1007/s00419-018-1363-0

ORIGINAL

Ahmad Paknejad · Gholamhossein Rahimi · Hamed Salmani

Analytical solution and numerical validation of piezoelectric energy harvester patch for various thin multilayer composite plates

Received: 19 August 2017 / Accepted: 6 March 2018 / Published online: 4 April 2018
© Springer-Verlag GmbH Germany, part of Springer Nature 2018

Abstract The study of vibrational energy harvesting using piezoelectric patch integrated on isotropic beam-like or plate-like thin structures has received significant attention over the past decade. Multilayer orthotropic composite plates are widely used in aerospace, automotive and marine applications, where they can be considered as host structures for vibration-based energy harvesting. In this paper, an exact analytical solution and numerical validation of a piezoelectric energy harvester structurally integrated to a thin multilayer orthotropic plate are presented. Electroelastic model of the thin multilayer composite plate with the piezoelectric patch harvester is developed based on a distributed parameter modeling approach with classical laminate plate theory assumptions for all-four-edge-clamped (CCCC) boundary condition. Closed-form steady-state expressions for coupled electrical outputs and structural vibration response are derived under harmonic transverse force excitation in the presence of a resistive load. Analytical electroelastic FRFs related to the voltage output as well as vibration response to force input are derived and generalized for different boundary conditions of host plate. The results of numerical and analytical models from multiple vibration modes are compared first for validating the analytical model with a case study employing a thin PZT-5A piezoceramic patch attached on the surface of a multilayer orthotropic composite CCCC plate. For this purpose, finite-element analysis is carried out by using ANSYS mechanical APDL software. Then, it is important to specify parameters in energy harvesting model, so positioning of piezoceramic patch harvester and excitation point force on the voltage output FRFs is discussed through an analysis of dynamic strain distribution on the overall plate surface. In addition, the effects of various composite laminate plates with different stacking sequences as host structures on generated power are discussed in details as well.

Keywords Smart composite plate · Electromechanical system · Piezoelectricity

1 Introduction

In the last few years there has been a growing interest in vibration-based energy harvesting to develop self-powered electrical output and wireless sensor monitoring systems [1,2], with the major goal of eliminating the need of battery replacement and disposal [2,4]. The power generated in this research fields is being achieved by applying required mechanical vibration from environment [5–7] or human activities [8,9]. In the literature, several transduction mechanisms have been proposed to convert ambient vibration into useful electrical energy such as the electrostatic [10,11], electromagnetic [12,13], magnetostrictive [14,15], piezoelectric [2–4] (as transduction principle conversion methods), as well as the use of electroactive polymers [16] and electrostrictive

A. Paknejad · G. Rahimi (✉) · H. Salmani
Department of Mechanical Engineering, Tarbiat Modares University, Tehran 14115-111, Iran
E-mail: rahimi_gh@modares.ac.ir
Tel.: (+9821) 8288-3356
Fax: (+9821) 8288-4909

polymers [17] (as alternative conversion techniques). Applying piezoelectric materials in energy harvesting comparing other transmit materials leads to higher power density, lighter weight, direct implementation, wider range of frequencies applications, ease of application as well as relative ease of fabrication to both micro- and macro-scaled devices. Despite electrostatic transduction, no bias voltage input is needed in piezoelectric transduction. Moreover, it is possible to exploit voltage directly from the material itself without step-up conversion [18,19].

In recent years, research on vibration-based energy harvesting is arguably focused on cantilever beam with unimorph or bimorph piezoelectric configurations. An exact analytical [20,21], semi-analytical [22], finite element [23,24], and nonlinear [25] electromechanical couple models of cantilevered unimorph/bimorph piezoelectric beam harvesters have been developed, and validated experimentally for harmonic [26] and random [27] transversely base excitations. Approximate analytical formulation of cantilever piezoelectric energy harvesters with axial deformations was accounted for Euler–Bernoulli, Rayleigh, and Timoshenko models [22]. Moreover, the study of bimorph configuration based on Timoshenko beam assumptions was investigated [28]. On the other hand, a significant number of studies have focused on numerical research [29–33]. For example, simple and complex structures include multiple modes of the system with the equivalent circuit model [29] as well as a linear system with a low natural frequency (non-buckled beam; and a buckled beam harvester) [30,31] were prepared different aspects of cantilever beam harvesters with optimization for size and shape of piezoceramic layers [32]. Note that, effect of enhancing the conversion abilities of piezoelectric materials derived based on initial energy injection [33]. Hence, major modeling issues [34] and performance enhancement of cantilevered beam harvesters has been widely studied for broadband base excitations with different design configurations to improve their energy harvesting characteristics [35–43]. For instance, the power generated from vibration is improved by exponentially tapered unimorph and bimorph cantilever piezoelectric with series and parallel connections [42]. It is worth pointing out that the case study of all these studies were considered isotropic single layer beam-like for host structure. Thereby, the study of cantilever bimorph piezoelectric with multilayer orthotropic beam was presented for different stacking sequence of host beam [43].

Integrating piezo-patch energy harvesters to plate-like structure eliminates the mass loading and volumetric occupancy of base-excited cantilever design [44]. Analytical model of a piezoelectric patch-based harvester attached on thin plates has been presented for harmonic [45] and random [46] transverse vibrations and for surface strain fluctuations of high impedance structures [47]. In addition, piezopatch-based energy harvesting from harmonic [48] and random [46] vibrations of thin plates were presented with electroelastic modeling, frequency-domain and time-domain solutions, as well as experimental investigations. Furthermore, analytical and numerical modeling of the equivalent circuit was explored for a piezo-patch energy harvester on a thin plate with AC–DC conversion [44]. Electromechanical finite-element model applicable to patch-based harvesters attached on thin plates was developed and extended to airflow excitation problems by electroaeroelastic coupling [49,50]. And also, topology optimization studies for distribution of piezoelectric materials on thin plates and shells were performed to maximize the generated power output [51].

Composite structures with high-strength, high-stiffness and lightweight properties are commonly used in numerous applications such as: automotive, hydrospace and aerospace [52]. Integrated piezoelectric patches sensors/actuators can easily be implemented for enabling self-monitoring and self-controlling. These advantages make them well suited for smart structure applications such as active vibration and buckling control, shape control, damage assessment, active noise control, structural health monitoring and energy harvesting [53]. The literature on piezoelectric patch-based energy harvesting attached on composite structure has focused on rectangular and nonrectangular bistable composite laminate plate [54,55]. The bistable composite laminate due to asymmetric stacking sequences can exhibit large deformation, and they have been identified as good candidates to integrate piezoelectrics for broadband energy harvesting [56,57]. Significant power outputs over a wide bandwidth have been obtained using bistable composite laminates due to the mismatch in thermal properties and the temperature change experienced during production [58]. The analytical, experimental and performance optimization study of bistable piezoelectric composite laminate for piezoelectric-based energy harvesting have been developed [59–63].

This work presents an exact analytical electroelastic model of piezoelectric patch energy harvester attached on thin multilayer orthotropic composite plate. For this purpose, the distributed parameter electroelastic model of a thin multilayer plate with a piezoelectric patch harvester is developed based on classical laminate plate theory and modal analysis procedure. Closed form expressions for the voltage, current, and power outputs as well as the mechanical response are presented for harmonic input. Numerical and analytical voltage FRF as well as peak voltage vs resistance are compared with a case study to show the accuracy of the analytical electroelastic model firstly. For this numerical analysis an APDL code is developed for the ANSYS software.

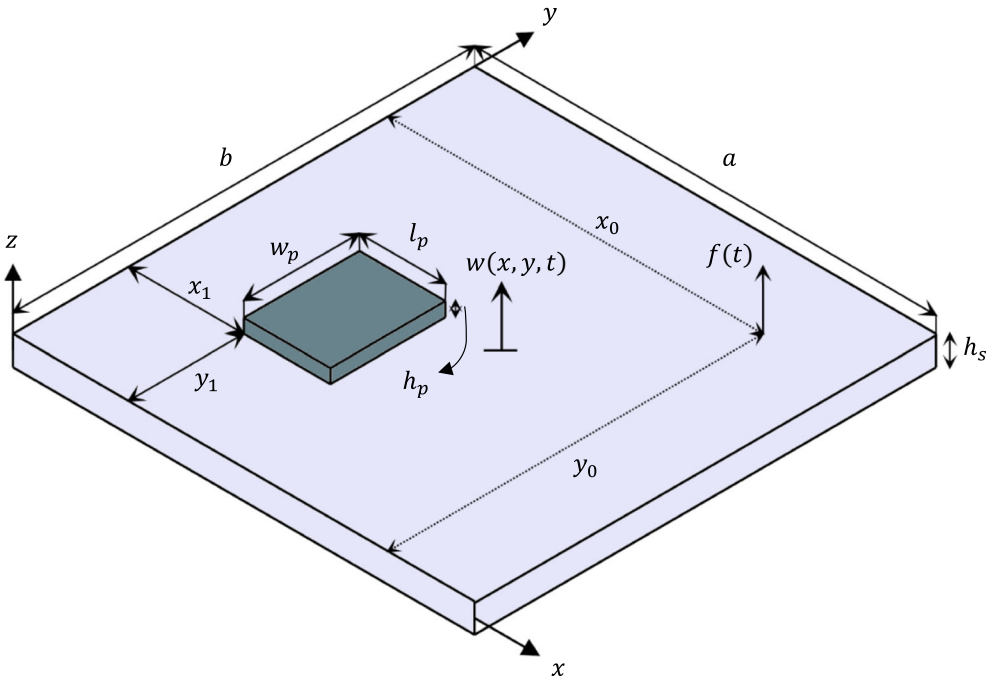

Fig. 1 The schematic of piezoelectric energy harvester integrated on composite host plate

Then, the exact normalized mode shapes of a CCCC multilayer plate are implemented to investigate the placement of harvester patch on the host plate for designing an efficient energy harvester model. Finally, energy harvesting from multiple vibration modes is analyzed and discussed extensively using analytical results. Note that this reliable analytical model can be used in design, performance prediction and power output optimization for energy harvesting from every thin multilayer and single-layer plates with either isotropic or orthotropic material properties employing integrated patch.

2 Analytical electroelastic modeling

In this section, the governing electroelastic equations of an energy harvester including composite plate as a substructure are developed in physical and modal coordinates. The mechanical and electrical coupled equations in physical coordinate are developed based on classical laminate plate theory, while the piezoelectric patch volume is assumed to be significantly smaller than the host plate. Therefore, the inertia and stiffness of piezoelectric patch are neglected because of their small effect on natural frequency and neutral axis. The schematic of the energy harvester is shown in Fig. 1, in which a small thin piezoelectric patch is bonded to a large multilayer composite plate with the length of a, width of b, and the thickness of h_{s}. The length, width and thickness of piezoelectric patch are specified by l_{p}, w_{p} and h_{p}, respectively. The plate is excited by transverse force $f\,(t)$ acting at the point (x_0, y_0).

2.1 Electroelastic formulation in physical coordinate

The governing equation of motion of a thin multilayer composite plate with piezoelectric patch is represented as

$$\frac{\partial^2\left(M_1^{\mathrm{s}}+M_1^{\mathrm{p}}\right)}{\partial x^2}+2\frac{\partial^2\left(M_6^{\mathrm{s}}+M_6^{\mathrm{p}}\right)}{\partial x\partial y}+\frac{\partial^2\left(M_2^{\mathrm{s}}+M_2^{\mathrm{p}}\right)}{\partial y^2}-R\frac{\partial}{\partial t}\left(\nabla^4 w\,(x,y,t)\right)$$
$$-C\frac{\partial w\,(x,y,t)}{\partial t}-m\frac{\partial^2 w\,(x,y,t)}{\partial t^2}+f\,(t)\,\delta\,(x-x_0)\,\delta\,(y-y_0)=0 \tag{1}$$

where superscripts "s" and "p" represent the substructure and piezoelectric patch, respectively. $w\,(x,y,t)$ is the transverse deflection at time (t) and location (x,y). The internal bending moments are M_1, M_2 along x

and y axis, and M_6 is the shear bending in $x-y$ plane. The Kelvin–Voigt damping as well as viscous damping coefficients are defined by R, C respectively, and m is the mass per unit area of the plate regardless of the mass effect of the piezoelectric patch. The location of point load $f(t)$ is defined by Dirac delta functions $\delta(x)$ and $\delta(y)$.

The internal bending moments of substructure are different in various directions due to orthotropic material properties of composite plate. Hence, the internal bending moments based on classical laminate plate theory are written in terms of curvature for host plate as follows

$$\begin{aligned} M_1^s &= D_{11}\kappa_x + D_{12}\kappa_y \\ M_2^s &= D_{12}\kappa_x + D_{22}\kappa_y \\ M_6^s &= 2D_{66}\kappa_{xy} \end{aligned} \tag{2}$$

where the mid-plane curvatures of the plate are represented as

$$\begin{aligned} \kappa_x &= -\frac{\partial^2 w(x,y,t)}{\partial x^2} \\ \kappa_y &= -\frac{\partial^2 w(x,y,t)}{\partial y^2} \\ \kappa_{xy} &= -\frac{\partial^2 w(x,y,t)}{\partial x \partial y} \end{aligned} \tag{3}$$

Substituting Eq. (3) into Eq. (2) gives the bending moments in terms of transverse deflection as follows

$$\begin{aligned} M_1^s &= -D_{11}\frac{\partial^2 w(x,y,t)}{\partial x^2} - D_{12}\frac{\partial^2 w(x,y,t)}{\partial y^2} \\ M_2^s &= -D_{12}\frac{\partial^2 w(x,y,t)}{\partial x^2} - D_{22}\frac{\partial^2 w(x,y,t)}{\partial y^2} \\ M_6^s &= -2D_{66}\frac{\partial^2 w(x,y,t)}{\partial x \partial y} \end{aligned} \tag{4}$$

where D_{11}, D_{22}, D_{12}, D_{66} are the bending stiffness along normal and shear direction, and are represented for k-th layer of multilayer host plate as [52]

$$\begin{aligned} D_{11} &= \frac{1}{3}\sum_{k=1}^{N} \bar{Q}_{11}^k \left(z_k^3 - z_{k-1}^3\right) \\ D_{12} &= \frac{1}{3}\sum_{k=1}^{N} \bar{Q}_{12}^k \left(z_k^3 - z_{k-1}^3\right) \\ D_{22} &= \frac{1}{3}\sum_{k=1}^{N} \bar{Q}_{22}^k \left(z_k^3 - z_{k-1}^3\right) \\ D_{66} &= \frac{1}{3}\sum_{k=1}^{N} \bar{Q}_{66}^k \left(z_k^3 - z_{k-1}^3\right) \end{aligned} \tag{5}$$

The above coefficients are usually simplified to $D_1 = D_{11}$, $D_2 = D_{22}$, $D_3 = D_{12} + 2D_{66}$. In Eq. (5), the $\bar{Q}$ parameters are determined as

$$\begin{aligned} \bar{Q}_{11} &= Q_{11}\cos^4\theta + 2(Q_{12} + 2Q_{66})\sin^2\theta\cos^2\theta + Q_{22}\sin^4\theta \\ \bar{Q}_{12} &= (Q_{11} + Q_{12} - 4Q_{66})\sin^2\theta\cos^2\theta + Q_{22}\left(\cos^4\theta + \sin^4\theta\right) \\ \bar{Q}_{22} &= Q_{11}\sin^4\theta + 2(Q_{12} + 2Q_{66})\sin^2\theta\cos^2\theta + Q_{22}\cos^4\theta \\ \bar{Q}_{66} &= (Q_{11} + Q_{22} - 2Q_{12} - 2Q_{66})\sin^2\theta\cos^2\theta + Q_{66}\left(\cos^4\theta + \sin^4\theta\right) \end{aligned} \tag{6}$$

in which,

$$Q_{11} = \frac{E_1}{1-\nu_{12}\nu_{21}}, \quad Q_{22} = \frac{E_2}{1-\nu_{12}\nu_{21}}$$
$$Q_{12} = \frac{\nu_{12}E_2}{1-\nu_{12}\nu_{21}}, \quad Q_{66} = G_{12} \tag{7}$$

The internal moments of the piezoelectric patch are defined as

$$M_1^{\mathrm{p}} = [H(x-x_1) - H(x-x_2)][H(y-y_1) - H(y-y_2)] \times \int_P T_1 z \mathrm{d}z$$
$$M_2^{\mathrm{p}} = [H(x-x_1) - H(x-x_2)][H(y-y_1) - H(y-y_2)] \times \int_P T_2 z \mathrm{d}z$$
$$M_6^{\mathrm{p}} = [H(x-x_1) - H(x-x_2)][H(y-y_1) - H(y-y_2)] \times \int_P T_6 z \mathrm{d}z \tag{8}$$

where $H(x)$ and $H(y)$ are Heaviside functions that can be specified the location of the piezoelectric patch in x and y directions, respectively. It should be noted that, for a thin piezoelectric patch attached on the host plate, the linear piezoelectric constitutive equations which are reduced to two dimensional (2D) from three dimensional (3D) can be written as [21]

$$\begin{bmatrix} T_1^{\mathrm{p}} \\ T_2^{\mathrm{p}} \\ T_6^{\mathrm{p}} \\ D_3 \end{bmatrix} = \begin{bmatrix} C_{11}^E & C_{12}^E & 0 & -e_{31} \\ C_{12}^E & C_{22}^E & 0 & -e_{31} \\ 0 & 0 & C_{66}^E & 0 \\ -e_{31} & -e_{31} & 0 & \varepsilon_{33}^{\mathrm{S}} \end{bmatrix} \begin{bmatrix} S_1^{\mathrm{p}} \\ S_2^{\mathrm{p}} \\ S_6^{\mathrm{p}} \\ E_3 \end{bmatrix} \tag{9}$$

where T_1, T_2 represent the normal stress components along x and y axes, respectively, T_6 is the shear stress in the $x-y$ plane, the electric displacement in z direction is D_3 (poling direction of piezoceramic patch), S_1^{p} and S_2^{p} exhibit the normal strain components along the x and y axes, S_6^{p} is the shear strain component in the $x-y$ plane, and E_3 is the electric field in the thickness direction. Also, e_{31} is the effective piezoelectric stress constant, $C_{11}^E = C_{22}^E$, C_{12}^E and C_{66}^E are the elastic stiffness components, and the permittivity component is $\varepsilon_{33}^{\mathrm{S}}$. Note that, superscript "p" represents the piezoceramic patch, while "E" and "S" denote the respective parameters which are determined at constant electric field and constant strain S, respectively. The reduced elastic, piezoelectric, and permittivity constants are

$$C_{11}^E = \frac{S_{11}^E}{\left(S_{11}^E + S_{12}^E\right)\left(S_{11}^E - S_{12}^E\right)}, \quad C_{12}^E = \frac{-S_{12}^E}{\left(S_{11}^E + S_{12}^E\right)\left(S_{11}^E - S_{12}^E\right)}, \quad C_{66}^E = \frac{1}{S_{66}^E}$$
$$e_{31} = \frac{d_{31}}{S_{11}^E + S_{12}^E}, \quad \varepsilon_{33}^{\mathrm{S}} = \varepsilon_{33}^T - \frac{2d_{31}^2}{S_{11}^E + S_{12}^E} \tag{10}$$

where S_{11}^E, S_{12}^E and S_{66}^E represent elastic compliance parameters at constant electric field E, d_{31} is the piezoelectric strain constant, and ε_{33}^T is the permittivity component at constant stress T.

The governing partial differential equation of the multilayer plate containing integrated piezoelectric patch is derived by substituting Eqs. (4) and (8) into Eq. (1) as follows

$$\begin{aligned} & D_1 \frac{\partial^4 w(x,y,t)}{\partial x^4} + 2(D_{12} + 2D_{66}) \frac{\partial^4 w(x,y,t)}{\partial x^2 \partial y^2} + D_2 \frac{\partial^4 w(x,y,t)}{\partial y^4} + R \frac{\partial}{\partial t}\left(\nabla^4 w(x,y,t)\right) \\ & + C \frac{\partial w(x,y,t)}{\partial t} + \rho_{\mathrm{s}} h_{\mathrm{s}} \frac{\partial^2 w(x,y,t)}{\partial t^2} - \chi v(t) \left\{ \left[\frac{\mathrm{d}\delta(x-x_1)}{\mathrm{d}x} - \frac{\mathrm{d}\delta(x-x_2)}{\mathrm{d}x} \right] [H(y-y_1) - H(y-y_2)] \right. \\ & \left. - [H(x-x_1) - H(x-x_2)] \left[\frac{\mathrm{d}\delta(y-y_1)}{\mathrm{d}y} - \frac{\mathrm{d}\delta(y-y_2)}{\mathrm{d}y} \right] \right\} \\ & = f(t)\,\delta(x-x_0)\,\delta(y-y_0) \end{aligned} \tag{11}$$

in which, $v(t)$ is the output voltage of the energy harvester, and χ is the electromechanical coupling term which is define as

$$\chi = e_{31} h_{\mathrm{pc}} \tag{12}$$

where h_{pc} is the distance of the piezoelectric mid-plane from neutral surface of the host plate. In this work, the piezoceramic patch's stiffness is neglected because its volume is assumed to be significantly smaller than the host plate. Therefore, the location of neural axis is considered to be in mid-plane of multilayer host plate even in the presence of piezoceramic patch in order to use classical laminate plate theory. Accordingly, the reference distance can be represented as

$$h_{\mathrm{pc}} = \frac{h_{\mathrm{s}} + h_{\mathrm{p}}}{2} \tag{13}$$

Due to the presence of two variables $v(t)$ and $w(x, y, t)$ in the governing electromechanical equation, another equation is needed to solve the problem. Hence, the electrical coupling equation is derived based on piezoelectric constitutive equation for thin plate as follows [45]

$$C_{\mathrm{p}} \frac{\mathrm{d}v(t)}{\mathrm{d}t} + \frac{v(t)}{R} + \chi \left\{ \int_{y_1}^{y_2} \int_{x_1}^{x_2} \left[\frac{\partial^3 w(x, y, t)}{\partial x^2 \partial t} + \frac{\partial^3 w(x, y, t)}{\partial y^2 \partial t} \right] \mathrm{d}x \mathrm{d}y \right\} = 0 \tag{14}$$

where R is the electric resistance and C_{p} is the electrical capacitance of piezoelectric patch which is defined as

$$C_{\mathrm{p}} = \left(\varepsilon_{33}^{\mathrm{S}} w_{\mathrm{p}} l_{\mathrm{p}} \right) / h_{\mathrm{p}} \tag{15}$$

Consequently, Eqs. (11) and (14) are the governing electroelastic equations of composite plate with a piezoelectric energy harvester in physical coordinates.

2.2 Electroelastic formulation in modal coordinate

In order to solve the governing Eqs. (11) and (14) using modal expansion method, it is needed to convert the equations in physical coordinate into modal coordinate. Accordingly, at first step, the multilayer host plate deflection equation is discretized into spatial and temporal distribution as follows:

$$w(x, y, t) = \sum_{m=1}^{\infty} \sum_{n=1}^{\infty} \phi_{mn}(x, y) \eta_{mn}(t) \tag{16}$$

where $\phi_{mn}(x, y)$ and $\eta_{mn}(t)$ are mass-normalized eigenfunction and modal time response for mn-th vibration mode, respectively. The mass-normalized eigenfunction ϕ_{mn} is different for various boundary condition. The eigenfunction of CCCC rectangular plate is expressed as follows [64]

$$\begin{aligned} \phi_{mn}(x, y) = C_{mn} & \left(\cos \lambda_{mn}^{x} x - \sigma_{mn}^{x} \sin \lambda_{mn}^{x} x - \cosh \mu_{mn}^{x} x + \frac{\lambda_{mn}^{x}}{\mu_{mn}^{x}} \sigma_{mn}^{x} \sinh \mu_{mn}^{x} x \right) \\ & \times \left(\cos \lambda_{mn}^{y} y - \sigma_{mn}^{y} \sin \lambda_{mn}^{y} y - \cosh \mu_{mn}^{y} y + \frac{\lambda_{mn}^{y}}{\mu_{mn}^{y}} \sigma_{mn}^{y} \sinh \mu_{mn}^{y} y \right) \end{aligned} \tag{17}$$

in which, the constants σ_{mn}^{x} and σ_{mn}^{y} are calculated as:

$$\sigma_{mn}^{x} = \frac{\cos \lambda_{mn}^{x} a - \cosh \mu_{mn}^{x} a}{\sin \lambda_{mn}^{x} a - \frac{\lambda_{mn}^{x}}{\mu_{mn}^{x}} \sinh \mu_{mn}^{x} a} \sigma_{mn}^{y} = \frac{\cos \lambda_{mn}^{y} b - \cosh \mu_{mn}^{y} b}{\sin \lambda_{mn}^{y} b - \frac{\lambda_{mn}^{y}}{\mu_{mn}^{y}} \sinh \mu_{mn}^{y} b} \tag{18}$$

and C_{mn} is the modal amplitude constant, which can be determined by normalizing the eigenfunctions by the following orthogonality conditions

$$\begin{aligned}\int_0^b\int_0^a \rho_s h_s \phi_{mn}(x,y)\,\phi_{rs}(x,y)\,\mathrm{d}x\mathrm{d}y = \delta_{mr}\delta_{ns}\int_0^b\int_0^a \Bigg(& D_1\frac{\mathrm{d}^2\phi_{mn}(x,y)}{\mathrm{d}x^2}\frac{\mathrm{d}^2\phi_{rs}(x,y)}{\mathrm{d}x^2} \\ &+ 2D_3\frac{\mathrm{d}^2\phi_{mn}(x,y)}{\mathrm{d}x^2}\frac{\mathrm{d}^2\phi_{rs}(x,y)}{\mathrm{d}y^2} \\ &+ D_2\frac{\mathrm{d}^2\phi_{mn}(x,y)}{\mathrm{d}y^2}\frac{\mathrm{d}^2\phi_{rs}(x,y)}{\mathrm{d}y^2}\Bigg)\mathrm{d}x\mathrm{d}y \\ = \omega_{mn}^2\delta_{mr}\delta_{ns}\end{aligned} \tag{19}$$

where δ_{mr} and δ_{ns} are Kronecker delta functions, which are equal to unity for $m = r$, $n = s$, and zero for $m \neq r$, $n \neq s$. The undamped natural frequency ω_{mn} for the mn-th vibration mode of the plate in short-circuit conditions is represented as

$$\omega_{mn} = \sqrt{\frac{D_1\left(\lambda_{mn}^x\right)^4 + 2D_3\left(\lambda_{mn}^x\right)^2\left(\lambda_{mn}^y\right)^2 + D_2\left(\lambda_{mn}^y\right)^4}{\rho_s h_s}} \tag{20}$$

The eigenvalues λ_{mn}^x, λ_{mn}^y, μ_{mn}^x and μ_{mn}^y are calculated by the simultaneous solution of the transcendental characteristic equations for CCCC B.C. shown in below [64]

$$\begin{aligned}\frac{1-\cos\lambda_{mn}^x a\times\cosh\mu_{mn}^x a}{\sin\lambda_{mn}^x a\times\frac{\lambda_{mn}^x}{\mu_{mn}^x}\sinh\mu_{mn}^x a} &= \frac{\left(\lambda_{mn}^x\right)^2-\left(\mu_{mn}^x\right)^2}{2\lambda_{mn}^x\mu_{mn}^x} \\ \frac{1-\cos\lambda_{mn}^y b\times\cosh\mu_{mn}^y b}{\sin\lambda_{mn}^y b\times\frac{\lambda_{mn}^y}{\mu_{mn}^y}\sinh\mu_{mn}^y b} &= \frac{\left(\lambda_{mn}^y\right)^2-\left(\mu_{mn}^y\right)^2}{2\lambda_{mn}^y\mu_{mn}^y}\end{aligned} \tag{21}$$

in which,

$$\begin{aligned}\mu_{mn}^x &= \sqrt{2\left(\lambda_{mn}^y\right)^2-\left(\lambda_{mn}^x\right)^2} \\ \mu_{mn}^y &= \sqrt{2\left(\lambda_{mn}^x\right)^2-\left(\lambda_{mn}^y\right)^2}\end{aligned} \tag{22}$$

For solving the characteristic equations based on the Newton's method, the needed intervals should be considered as

$$\begin{aligned}\lambda_{mn}^x a &\in \left[m\pi,\ m\pi+\frac{\pi}{2}\right],\quad m=1,2,\ldots \\ \lambda_{mn}^y b &\in \left[n\pi,\ n\pi+\frac{\pi}{2}\right],\quad n=1,2,\ldots\end{aligned} \tag{23}$$

Substituting Eq. (16) into Eq. (11), and integrating it at the plate domain after multiplying it by $\phi_{mn}(x,y)$, and employing orthogonality conditions of Eq. (19), the electromechanically coupled ordinary differential equation of the multilayer plate in modal space is derived as

$$\frac{\mathrm{d}^2\eta_{mn}}{\mathrm{d}t^2} + 2\zeta_{mn}\omega_{mn}\frac{\mathrm{d}\eta_{mn}}{\mathrm{d}t} + \omega_{mn}^2\eta_{mn}(t) - \chi_{mn}v(t) = f_{mn}(t) \tag{24}$$

where ζ_{mn} is the modal damping ratio. In Eq. (24), $f_{mn}(t)$ and χ_{mn} are modal forcing and electromechanical coupling terms, and are defined as

$$\begin{aligned}f_{mn}(t) &= \int_0^b\int_0^a f(t)\,\delta(x-x_0)\,\delta(y-y_0) \\ \phi_{mn}(x,y)\,\mathrm{d}x\mathrm{d}y &= f(t)\,\phi_{mn}(x_0,y_0) \\ \chi_{mn} &= \chi\left[\int_{y_1}^{y_2}\frac{\partial\phi_{mn}(x,y)}{\partial x}\Bigg|_{x_1}^{x_2}\mathrm{d}y + \int_{x_1}^{x_2}\frac{\partial\phi_{mn}(x,y)}{\partial y}\Bigg|_{y_1}^{y_2}\mathrm{d}x\right]\end{aligned} \tag{25}$$

In order to obtain the second governing equation in modal space, the modal expansion given by Eq. (16) is substituted into Eq. (14) as follows

$$C_{\mathrm{p}}\frac{\mathrm{d}v\,(t)}{\mathrm{d}t}+\frac{v\,(t)}{R}+\sum_{n=1}^{\infty}\sum_{m=1}^{\infty}\chi_{mn}\frac{\mathrm{d}\eta_{mn}\,(t)}{\mathrm{d}t}=0 \tag{26}$$

Therefore, two governing equations for piezoelectric energy harvester embedded on composite plate are transferred into modal space. Finally, the closed form steady-state formulations will be obtained in the next section based on these two equations of motion.

2.3 Steady-state solution under harmonic excitation

For steady-state solution, transverse force is assumed to be harmonic, i.e., $f\,(t)=F_0\mathrm{e}^{j\omega t}$, where F_0 is the force amplitude and ω is the excitation frequency. According to assumption of the harmonic force excitation and linear oscillations, the steady-state expressions for voltage response $v\,(t)$ and modal response $\eta_{mn}\,(t)$ can be expressed as

$$\begin{aligned} v\,(t)&=V_0\mathrm{e}^{j\omega t}\\ \eta_{mn}\,(t)&=H_{mn}\mathrm{e}^{j\omega t}\end{aligned} \tag{27}$$

Substituting Eq. (27) into the electromechanical coupled governing Eqs. (24) and (26), the complex amplitudes V_0 and H_{mn} are determined as

$$\begin{aligned} H_{mn}&=\frac{F_0\phi_{mn}\,(x_0,\,y_0)-\chi_{mn}V_0}{\omega_{mn}^2-\omega^2+2j\zeta_{mn}\omega_{mn}\omega}\\ V_0&=\frac{-j\omega\sum_{n=1}^{\infty}\sum_{m=1}^{\infty}\frac{F_0\phi_{mn}(x_0,y_0)\chi_{mn}}{\omega_{mn}^2-\omega^2+2j\zeta_{mn}\omega_{mn}\omega}}{\frac{1}{R}+j\omega\,C_{\mathrm{p}}+j\omega\sum_{r=1}^{\infty}\frac{j\omega\,\chi_{mn}^2}{\omega_{mn}^2-\omega^2+2j\zeta_{mn}\omega_{mn}\omega}}\end{aligned} \tag{28}$$

Hence, the closed form steady-state responses for voltage $v\,(t)$ across the resistive load, the electric current $i\,(t)=v\,(t)/R$ and instantaneous power output $p\,(t)=v\,(t)^2/R$ generated by piezoceramic patch can be written as

$$v\,(t)=V_0\mathrm{e}^{j\omega t}=\left(\frac{-j\omega\sum_{n=1}^{\infty}\sum_{m=1}^{\infty}\frac{F_0\phi_{mn}(x_0,y_0)\chi_{mn}}{\omega_{mn}^2-\omega^2+2j\zeta_{mn}\omega_{mn}\omega}}{\frac{1}{R}+j\omega\,C_{\mathrm{p}}+j\omega\sum_{r=1}^{\infty}\frac{j\omega\,\chi_{mn}^2}{\omega_{mn}^2-\omega^2+2j\zeta_{mn}\omega_{mn}\omega}}\right)\mathrm{e}^{j\omega t} \tag{29}$$

$$i\,(t)=i_0\mathrm{e}^{j\omega t}=\left(\frac{1}{R}\times\frac{-j\omega\sum_{n=1}^{\infty}\sum_{m=1}^{\infty}\frac{F_0\phi_{mn}(x_0,y_0)\chi_{mn}}{\omega_{mn}^2-\omega^2+2j\zeta_{mn}\omega_{mn}\omega}}{\frac{1}{R}+j\omega\,C_{\mathrm{p}}+j\omega\sum_{r=1}^{\infty}\frac{j\omega\,\chi_{mn}^2}{\omega_{mn}^2-\omega^2+2j\zeta_{mn}\omega_{mn}\omega}}\right)\mathrm{e}^{j\omega t} \tag{30}$$

$$p\,(t)=P_0\left(\mathrm{e}^{j\omega t}\right)^2=\left(\frac{1}{R}\times\left(\frac{-j\omega\sum_{n=1}^{\infty}\sum_{m=1}^{\infty}\frac{F_0\phi_{mn}(x_0,y_0)\chi_{mn}}{\omega_{mn}^2-\omega^2+2j\zeta_{mn}\omega_{mn}\omega}}{\frac{1}{R}+j\omega\,C_{\mathrm{p}}+j\omega\sum_{r=1}^{\infty}\frac{j\omega\,\chi_{mn}^2}{\omega_{mn}^2-\omega^2+2j\zeta_{mn}\omega_{mn}\omega}}\right)^2\right)\left(\mathrm{e}^{j\omega t}\right)^2 \tag{31}$$

Finally, the transverse deflection is calculated by substituting the modal and voltage response Eqs. (27) and (28) into vibration response given by Eq. (16) as

$$\begin{aligned} w\,(x,\,y,\,t)=\sum_{n=1}^{\infty}\sum_{m=1}^{\infty}&\left(\phi_{mn}\,(x_0,\,y_0)-\frac{-j\omega\sum_{n=1}^{\infty}\sum_{m=1}^{\infty}\frac{\phi_{mn}(x_0,y_0)\chi_{mn}}{\omega_{mn}^2-\omega^2+2j\zeta_{mn}\omega_{mn}\omega}}{\frac{1}{R}+j\omega\,C_{\mathrm{p}}+j\omega\sum_{r=1}^{\infty}\frac{j\omega\,\chi_{mn}^2}{\omega_{mn}^2-\omega^2+2j\zeta_{mn}\omega_{mn}\omega}}\right)\\ &\times\frac{F_0\phi_{mn}\,(x,\,y)\,\mathrm{e}^{j\omega t}}{\omega_{mn}^2-\omega^2+2j\zeta_{mn}\omega_{mn}\omega}\end{aligned} \tag{32}$$

Closed-form steady-state expressions for electrical (voltage, current and power) and mechanical vibration (deflection) responses have been derived. As it can be seen, the ability of using present model which was obtained based on classical laminate plate theory is to analyze the energy generated from active element attached on multilayer orthotropic substructures. It means that the present formulations cover a large range of engineering structures from l-layer to multilayer structures with isotropic or orthotropic material properties and different stacking sequences of each layer.

3 Validation

In this section, validation for the proposed mathematical model is presented based on simple model of substructure like 1-layer isotropic plate. For this purpose, the analytical results of Aridogan et al. [45] for the structurally integrated piezoceramic patch harvester from multiple vibration modes are used as benchmark. Aridogan model [45] applied an analytical approach based on the Kirchhoff's plate theory which is made just for 1-layer isotropic plate; however, the classical laminate plate theory assumptions which have extended Kirchhoff's assumptions for orthotropic or even for composite multilayer thin plates were exploited in previous section. The advantage of using present theory is that thin isotropic, orthotropic or laminate plates with constant or widthwise variable material properties of substructure can be considered in the extracted analytical formulations. It should be noted that a separate Code is built in MATLAB in order to reconstruct the electromechanical model of Aridogan [45]. In addition, the output voltage of present model is calculated based on Eq. (29) for isotropic material properties as $E_1 = E_2 = E,\ \vartheta = \vartheta_{12} = \vartheta_{21},\ G_{12} = E/2\,(1+\vartheta)$. All of input parameters including material properties, dimensions as well as configuration were chosen the same as those ones in Aridogan [45]. For compassion purpose, Fig. 2 shows the voltage FRF of the 2 different models, and also, Fig. 3 shows the variations of the voltage amplitude with load resistance for the first vibration mode of 2 different models.

According to Fig. 2, the result of voltage FRF for the present model shows an excellent match with Aridogan [45]. Table 1 shows comparison of 2 different models for natural frequencies as well as maximum output voltage for the first four resonances. Furthermore, the results of 2 different models are almost coincide as shown in Fig. 3, it can be seen that it is difficult to distinguish.

It can be concluded that the derived formulations in the present study work very well for a simple case study which was contained one-layer isotropic plate for its substructure. Now, it is time to see the results of energy generated from piezoelectric patch attached on multilayer composite plate with orthotropic material properties and different stacking sequences.

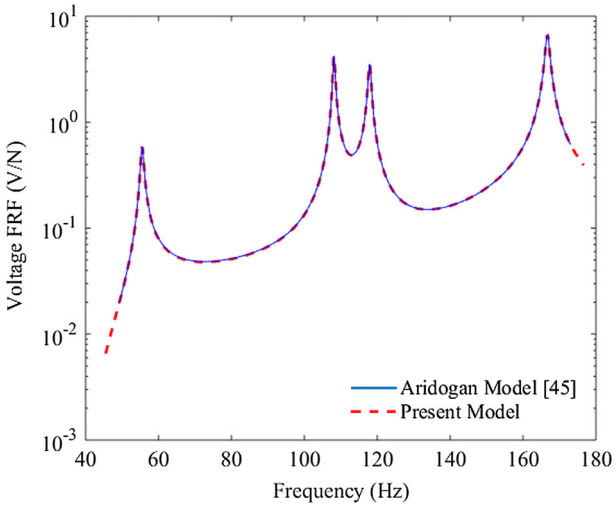

Fig. 2 Voltage FRF at $R = 1180$ and configuration from [45]

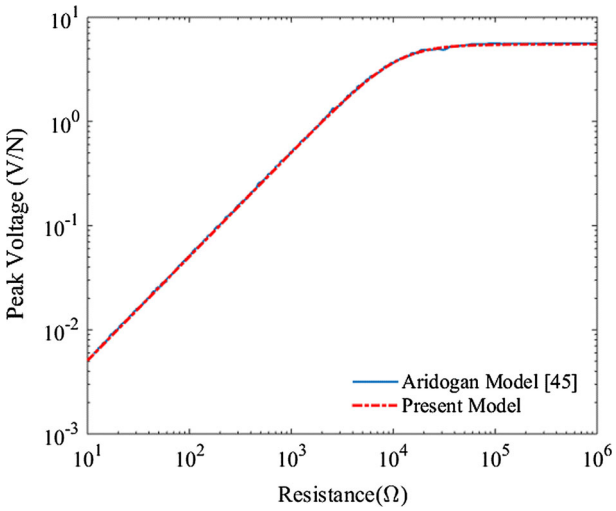

Fig. 3 Peak voltage versus resistance for the first resonance at 55.4 Hz and configuration from Ref. [45]

Table 1 Natural frequency/output voltage

Parameter	Aridogan [45]	Present Model
First mode	$\frac{55.492}{0.5866}$	$\frac{55.512}{0.5853}$
Second mode	$\frac{108.132}{4.22}$	$\frac{108.143}{4.19}$
Third mode	$\frac{117.922}{3.547}$	$\frac{117.903}{3.526}$
Fourth mode	$\frac{166.696}{6.674}$	$\frac{166.678}{6.689}$

4 Results and discussions

In this section, examples are solved to show the performance of the developed analytical formulations of the multilayer composite plate with piezoelectric energy harvester. Regarding the lack of results on experimental or numerical study of multilayer plate with piezoelectric energy harvester patch in the literature, a numerical solution is performed first to verify the developed analytical formulation. It should be noted that in the case of a structurally integrated piezoelectric energy harvester on a thin plate, the piezoelectric patch location and excitation force position have significant effects on the performance of the collected charge output on the electrodes of the harvester. Therefore, after verification, positioning of piezoelectric and excitation force on the host plate is analyzed with a case study. Then, some parameters are studied to investigate their effects on the performance of energy harvester.

In these examples, four different types of multilayer composite plates including TC1, TC2, TC3, and TC4 with different stacking sequences are considered in details as host structures. It is worth pointing out that the material and geometric properties of these different substructures are chosen the same to have better conclusion. The orthotropic material properties of carbon/epoxy [65] shown in Table 2 as well as the geometric properties listed in Table 3 are used for each layer of these 8-layer composite plates. Furthermore, the boundary conditions of the host plates are assumed to be four-edge-clamped (CCCC) for all case studies. Also, the piezoceramic patch is assumed to be PZT-5A with material properties of Table 4 and the dimensions considered in Table 5.

One of the most important parameters in vibration-based energy harvesting is modal damping ratio ζ_{mn}. According to the literature for most similar case studies, the damping ratio is defined as $0.009 \pm 5e{-}4$, $0.006 \pm 5e{-}4$ for the first two resonances, respectively. Consequently in the present work, this parameter can be assumed to be 0.009, 0.006 for the first and second modes, respectively. It should be noted that the values of this parameter are chosen to show the performance of extracted analytical formulations with the effects of damping ratio coefficients. Also, the damping ratio coefficients for other natural frequencies, due to the impact of Kelvin–Voigt (R) as well as viscosity damping (C) can be defined according to Eq. (24) as

Table 2 Material properties of carbon/epoxy lamina [65]

Parameters	Unit	Value
E_{11}	GPa	108
$E_{22} = E_{33}$	GPa	10.3
$G_{12} = G_{13}$	GPa	7.13
G_{23}	GPa	4.02
$\upsilon_{12} = \upsilon_{13}$		0.28
υ_{23}		0.0267
ρ	kg/m^3	1530

Table 3 Dimensions of host plate

Type	Length (mm)	Width (mm)	Thickness of each layer (mm)
$[0, 90, 0, 90]\,s$ − TC1 $[30, -30, 30, -30]\,s$ − TC2 $[45, -45, 45, -45]\,s$ − TC3 $[60, -60, 60, -60]\,s$ − TC4	580	540	0.4

Table 4 PZT-5A material properties

Parameter	Unit	Value
C_{11}	GPa	120.35e9
C_{12}		75.18e9
C_{13}		75.09e9
C_{33}		110.87e9
C_{44}		21.05e9
C_{55}		21.05e9
C_{66}		22.57e9
e_{31}	pm/V	− 9.06
e_{33}		12.93
e_{15}		12.29
ε_r	nF/V	8.854e−12
ε^s_{11}		$1730\varepsilon_r$
ε^s_{22}		$1730\varepsilon_r$
ε^s_{33}		$1700\varepsilon_r$

Table 5 Dimensions of piezoceramic patch

Type	Length (mm)	Width (mm)	Thickness (Mm)	
			For analytical results sections 3.2, 3.3	For numerical validation section 3.1
PZT-5A	72.4	72.4	0.26	0.6

$$\zeta_{mn} = C_R \omega_{mn} + \frac{C_C}{\omega_{mn}} \tag{33}$$

where C_R, C_C are constant coefficients related to Kelvin–Voigt (R) and viscosity damping (C), respectively. For each case studies shown in Table 3, these constant coefficients will be obtained by having the damping coefficients ζ_{mn} and natural frequency ω_{mn} for the first two natural frequencies.

4.1 Numerical verification

Before entering the parametric study, in order to refine the confidence, the result from the developed analytical model is compared with multilayer composite plate using finite-element method. For this purpose, an example of piezoceramic patch harvester attached on a thin multilayer composite TC1 is solved for all-four-edge-clamped (CCCC) boundary condition. For analytical solution, the voltage output from Eq. (29) is calculated

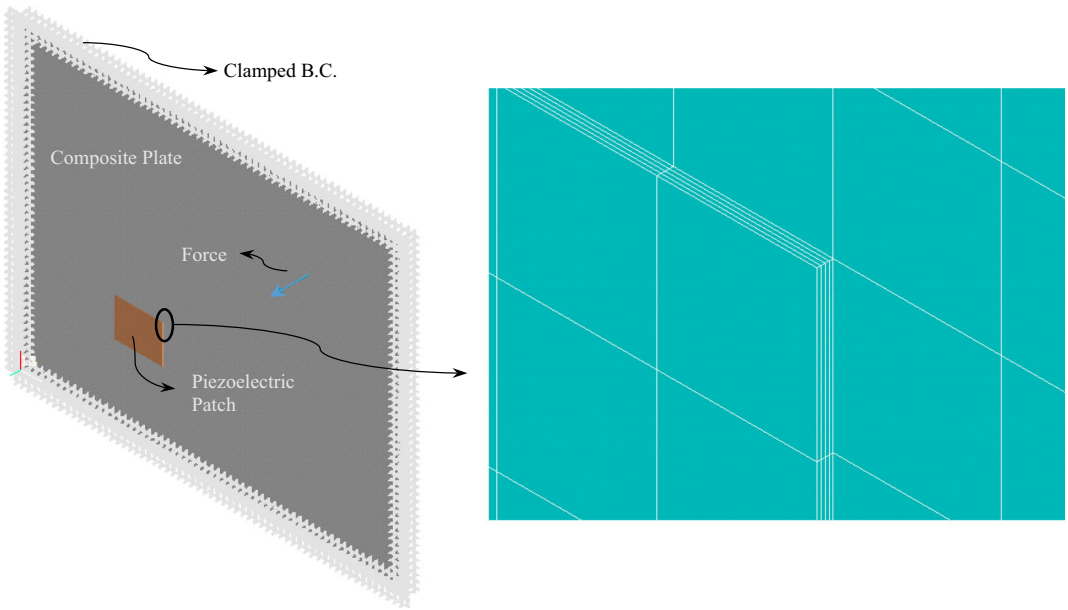

Fig. 4 Finite-element model of multilayered piezoelectric energy harvester

Table 6 Natural frequencies and damping ratio coefficients

Parameter	Natural frequencies (Hz)		Error %	Damping ratio
	Analytical	Numerical		
First mode	95.10	94.33	0.82	0.009
Second mode	183.41	182.67	0.41	0.006
Third mode	207.93	206.30	0.79	0.0057
Fourth mode	270.99	269.16	0.68	0.0055

with the double summation m from 1 to 2 and n from 1 to 2 for the first four natural frequencies including 50–300 Hz. Also for numerical solution, an APDL code is developed for the ANSYS software in order to model piezoelectric energy harvesting based on harmonic excitation. Advantage of ANSYS is its ability to analyze piezoelectric material as well as electric resistance. The host multilayer plate and piezoceramic patch are modeled by solid continuum elements SOLID185 and SOLID5, respectively. In addition, to perform the modeling piezoelectric energy harvester the CIRCU94 element is implemented to create electrical resistance. In this example, the electrical resistance is taken to be 1000 Ω. Furthermore, the piezoceramic patch and excitation force locations are assumed to be place at $(x_1, y_1) = (0.165, 0.155)$ and $(x_0, y_0) = (0.165, 0.385)$, respectively. It is worth pointing out that the values of the piezoceramic patch and excitation force locations used in this analysis are taken arbitrarily to observe the general trends between analytical and numerical results. A typical three-dimensional finite-element model and mesh are shown in Fig. 4.

The first four natural frequencies which are obtained from both analytical and numerical solutions are listed in Table 6; hence, the modal damping coefficients shown in Table 6 can be determined based on these resonances and Eq. (33).

The output voltage FRF generated out of the piezoelectric patch from finite-element method are compared with the analytical solutions in Fig. 5. The analytical voltage FRFs exhibit very good agreement with numerical result especially near the resonance frequencies. According to the results shown in Table 7, the difference of two compared methods is less than 2.5% for first and third modes, and 4.07 and 3.34% for second and fourth modes, respectively. In addition, the numerical result of peak voltage versus load resistance is compared with analytical one as shown in Fig. 6. At the fourth resonance frequency, it can be seen that the difference between analytical and numerical results is insignificant for a wide range of load resistance (10−10e6 Hz).

It means that the current analytical formulation well predicts the piezoelectric energy harvester's behavior. Having shown the accuracy of the proposed analytical model, some parameters are studied in the next sections

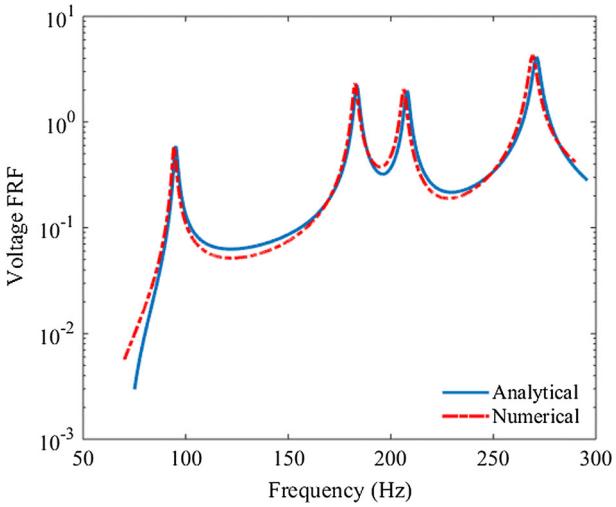

Fig. 5 Comparison of the numerical and analytical voltage FRFs for a load resistance of 1 kΩ

Table 7 Results output analytical and numerical solutions

Parameter	Output voltage (V)		Error %
	Analytical	Numerical	
First mode	0.5911	0.5816	1.63
Second mode	2.218	2.312	4.07
Third mode	1.984	2.032	2.36
Fourth mode	4.141	4.284	3.34

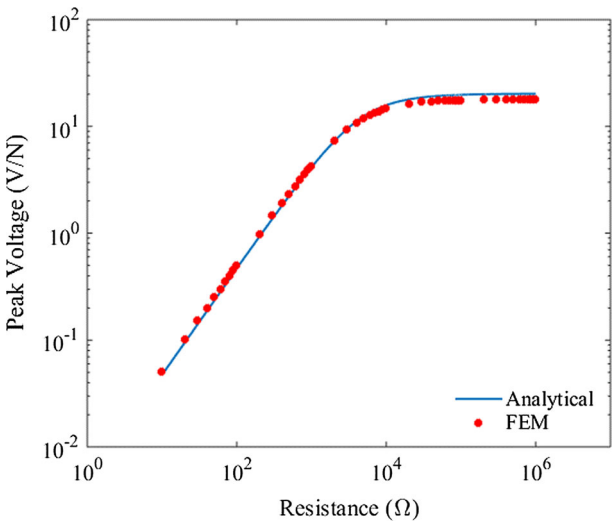

Fig. 6 Comparison of the numerical and analytical peak voltage versus load resistance at fourth resonance

to analyze their effects on output voltage and power generated from piezoelectric energy harvester attached on multilayer host plate.

4.2 Piezoelectric and force locations

For designing an efficient piezoelectric energy harvester, it is necessary to find the best location for the excitation force and piezoelectric patch. It is obvious that the deflection and strain distribution is different in various mode

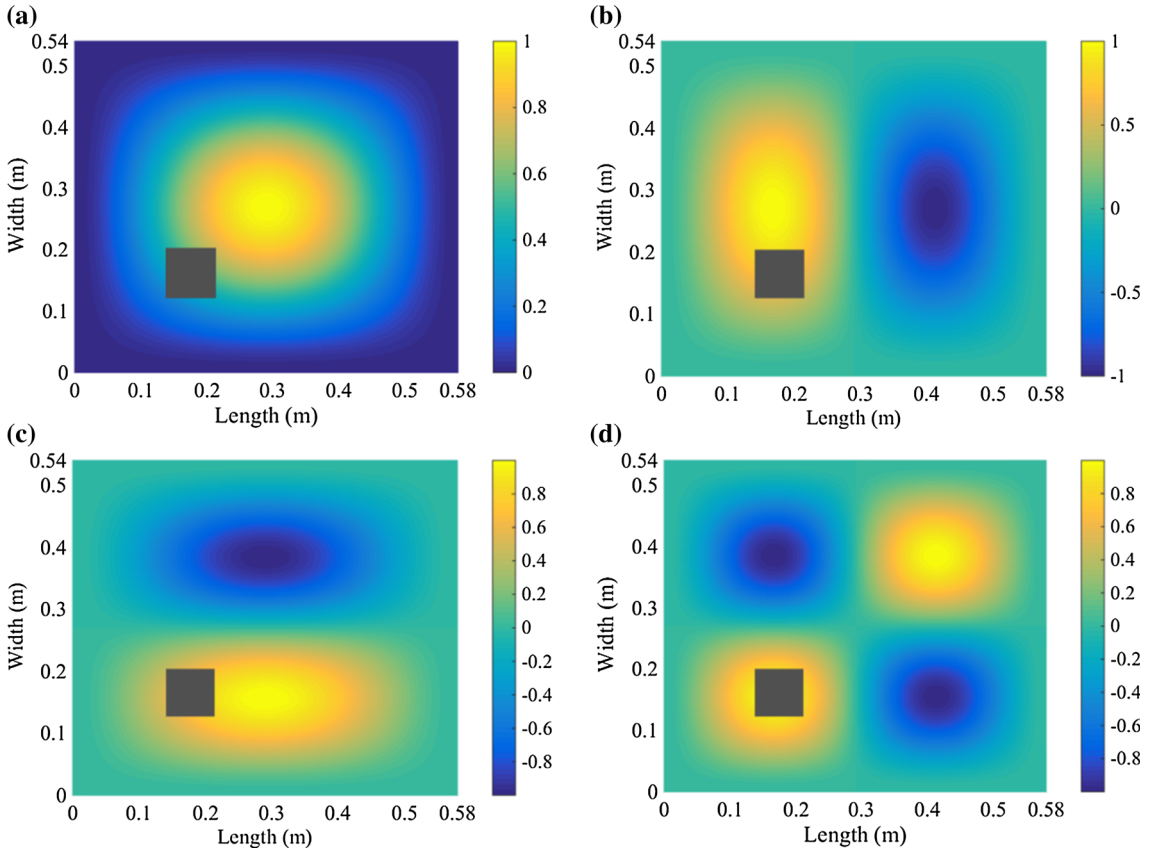

Fig. 7 Normalized mode shapes of composite TC1 for **a** first, **b** second, **c** third, and **d** fourth mode

shapes, and the maximum voltage is produced in a particular place with the maximum strain changes based on the piezoelectric effect that can generate an electric charge in response to applied mechanical stress. It should be noted that in the present work, the ultimate goal is study of energy generated for a broad range of frequency stimulation including at least four or more natural frequencies.

The first four normalized mode shapes of composite plate TC1 including (1, 1), (1, 2), (2, 1) and (2, 2) are shown for the clamped boundary condition in Fig. 7. According to Fig. 7a the fundamental mode (1, 1) of the free vibration is a single sine wave in the x and y directions with the natural frequency $\omega_{11} = 95.1$ Hz. The normalized maximum strain point is at center of the plate. The deflected surfaces that correspond to second and third modes of (1, 2), (2, 1) with the natural frequencies $\omega_{12} = 183.41$ Hz, $\omega_{21} = 207.93$ Hz are displayed in Fig. 7b, c, respectively. There are two points with maximum strains and one symmetry line along the center of x or y axis for the second (1, 2) and third (2, 1) mode shapes, respectively. Finally, the fourth mode of (2, 2) with the natural frequency $\omega_{22} = 270.98$ Hz which is shown in Fig. 7d has four symmetric maximum strains points and the nodal lines along the center of both x and y directions.

Based on the foregoing paragraphs, nodal lines are the points remaining at rest, and have zero strain. Therefore, the power generated from piezoelectric patch which is placed on the nodal line is closed to zero. According to the reference [45] and Fig. 7, there are four different domains where are far enough from nodal lines, so the optimal placements of piezoelectric patch are near the center of quadrant of the plate to harvest energy from multi vibration modes of the plate. Finally in this work, the piezoceramic patch which is shown with a black square is placed at the left-lower quadrant of the host plate $(x_1, y_1) = \left(\frac{0.58}{4}, \frac{0.54}{4}\right) = (0.165, 0.155)$. The schematic and geometry of final model are shown in Fig. 8.

In order to complete energy harvesting model, it is needed to find the best location for excitation point force. Therefore, tuning the location of excitation point force shown in Fig. 9 is done by calculating maximum voltage output from the first four natural frequency including 50–300 Hz for different force position on composite plate TC1. As shown in Fig. 9, there are four excitation point force locations on the host plate that generate

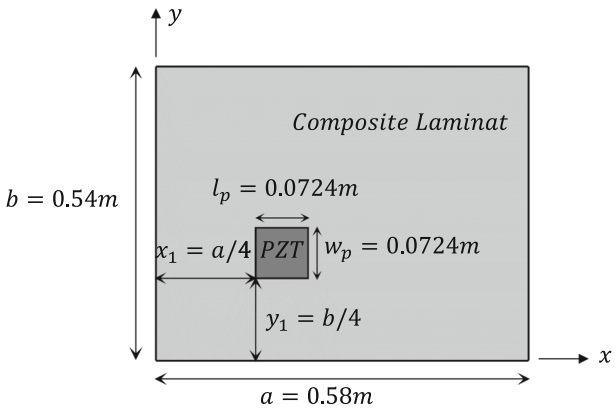

Fig. 8 Schematic of piezoelectric patch and structural host plate with geometric properties

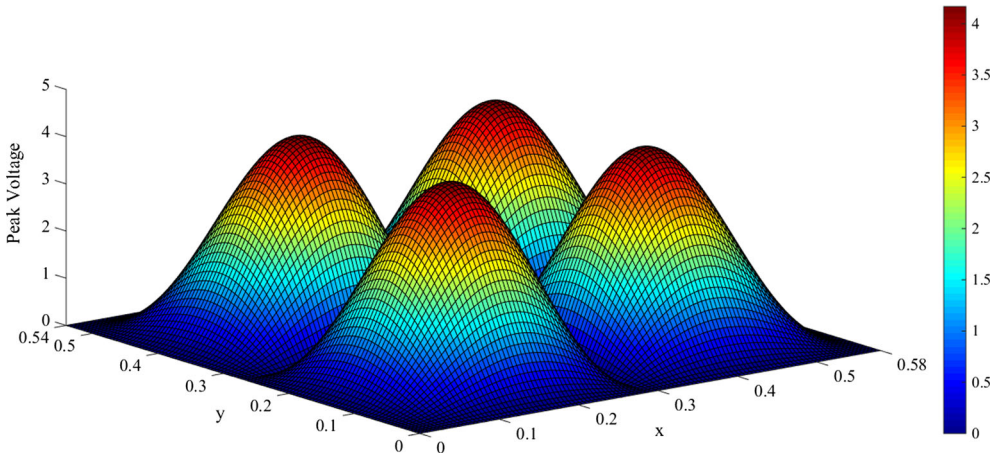

Fig. 9 Maximum output voltage among the first four natural frequency of host composite plate TC1 for different excitation point force position

Table 8 The points which is generate maximum voltage output

No.	*x*	*y*
1	0.165	0.155
2	0.415	0.155
3	0.415	0.385
4	0.165	0.385

maximum output voltage. These points are presented in Table 8, and their effects on output voltage are depicted in Fig. 10.

Interestingly, the voltage frequency–response curve for excitation points Nos. 1, 2, and 3 includes seven resonances and at least three anti-resonances. However, the only one anti-resonance can be seen in the voltage frequency–response curve of excitation point force No. 4. Obviously, the number of anti-resonances depends on excitation point force location on the host structure. Therefore, evaluating the results shows that setting the excitation force at the point No. 4 leads to extracting higher voltage along the first seven natural frequencies from the energy harvester. Furthermore, it is more advantageous for a designer to set the force location in an optimal placement to have minimums before and after the exciting frequency in FRF diagram. It is just because the output voltage is dramatically dropped just before and after the natural frequencies, when it is between two anti-resonances.

Finally, after specifying the piezoelectric patch location and excitation force position on the host plate, the model of multilayer plate with piezoelectric patch harvester is completed. Therefore, the electromechanical

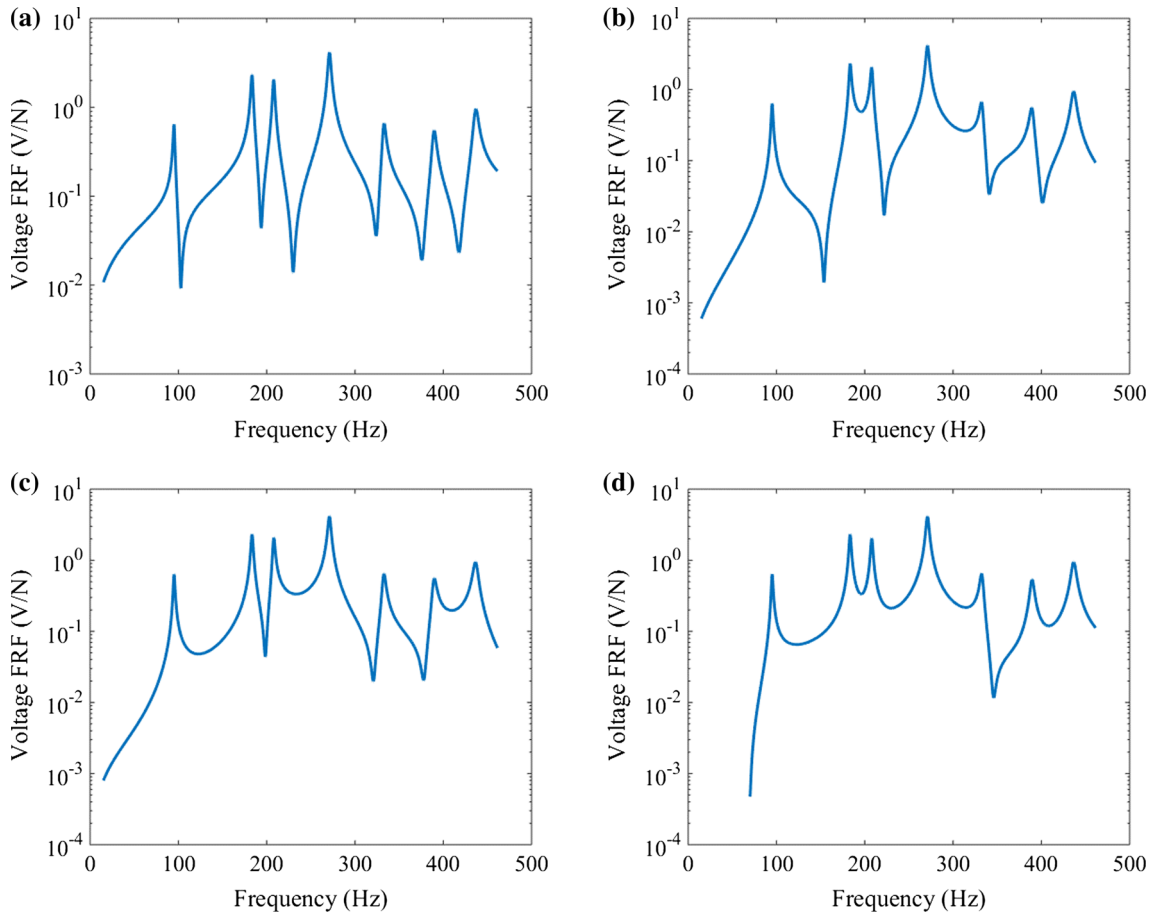

Fig. 10 Voltage FRFs for excitation point force **a** No. 1, **b** No. 2, **c** No. 3, and **d** No. 4 based on host composite plate TC1

results which exhibit the performance of piezoceramic patch on multilayer host plate analytically are analyzed and discussed as well in the next section.

4.3 Electromechanical result

In this section, the parametric study of the electromechanical results for multilayer host plate with piezoceramic patch energy harvester is presented based on applying the analytical developed solution in two categories. The effect of changing stacking sequence of multilayer host plate on power generated is studied in the first group of diagrams. Furthermore, the frequency responses of piezoelectric patch harvester on isotropic host plate are also presented to show the differences of output voltage with an orthotropic one. The second group of results includes the voltage, current and power FRFs for various resistive load. In addition, the variation of generated peak voltage, current and power in the term of resistance are shown in this group of results. The results of second category are obtained for a special composite plate (TC1).

4.3.1 Group A: effect of various stacking sequence

In this group of results, the generated power which is the most important output in energy harvesting design parameters is analyzed in details for different composite plates with various type of stacking sequence TC1, TC2, TC3, and TC4. For the first four vibration modes of each composite plates, the natural frequencies which are obtained from analytical solution and damping ratio coefficients which can be calculated based on Eq. (33) are shown in Table 9.

Table 9 Natural frequency/damping ratio

Type	Mode 1	Mode 2	Mode 3	Mode 4
$[0, 90, 0, 90]\,s$ − TC1	95.10/0.009	183.41/0.006	207.93/0.0057	270.99/0.0055
$[30, -30, 30, -30]\,s$ − TC2	92.55/0.009	162.38/0.006	209.28/0.0053	286.59/0.0049
$[45, -45, 45, -45]\,s$ − TC3	94.62/0.009	183.70/0.006	197.20/0.0058	298.63/0.0056
$[60, -60, 60, -60]\,s$ − TC4	97.85/0.009	157.57/0.006	232.46/0.0046	299.59/0.0041

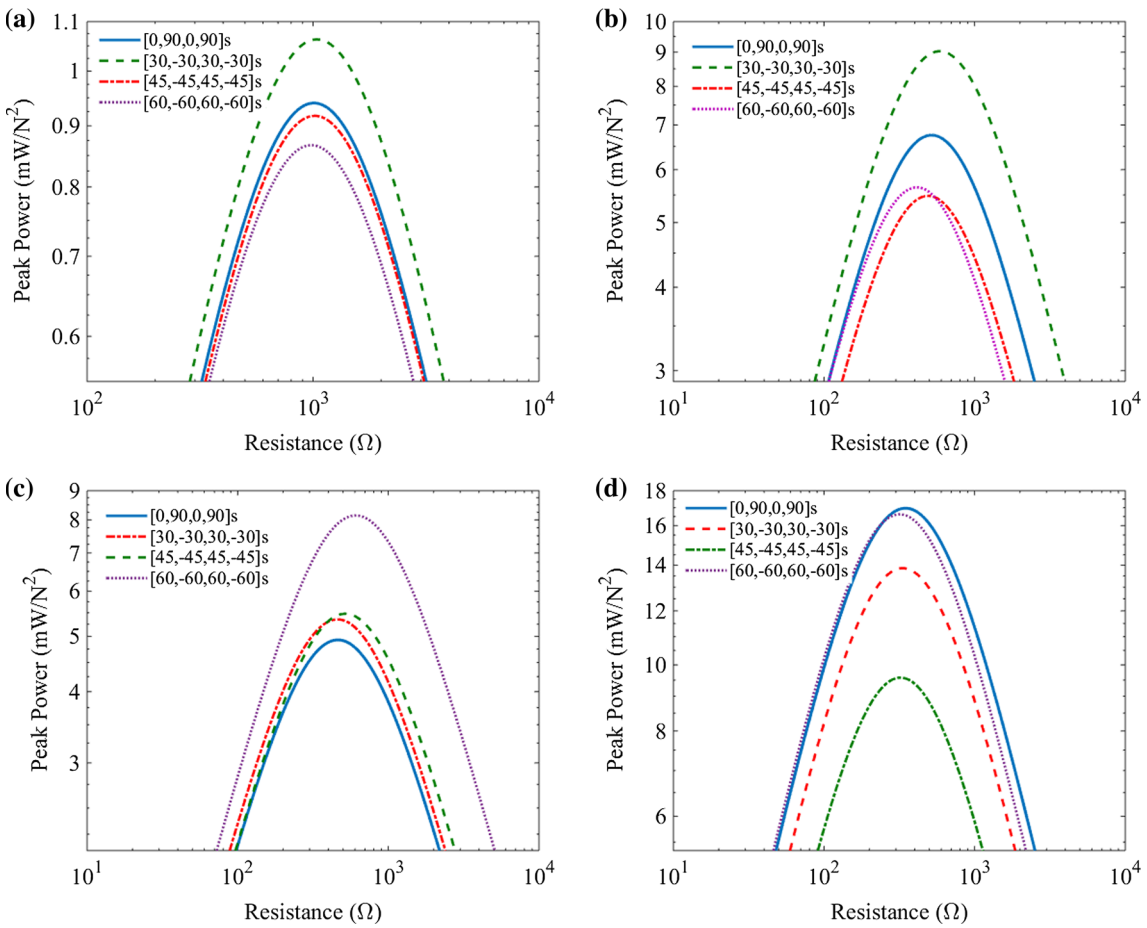

Fig. 11 Variation of peak output power at **a** first; **b** second; **c** third and **d** fourth mode frequency versus load resistance for different composite laminate host plate

Actually, mode shapes of various plates remain almost constant with changing stacking sequence of host plate. However, the dynamic parameters including deflections, strains, and natural frequencies of these plates especially in the peaks have significant changes in quantitative term. Therefore, piezoelectric patch is placed under different strain changes sign, and generate different electrical power. Variations of peak power amplitudes at the first four vibration modes are plotted versus resistance load for different types of composite laminate host plate in Fig. 11.

According to Fig. 11, as it is expected, all of maximum output power among the sample values of different composite plate in each mode occurred around the same resistant load. This results show that the composite laminated plates with different stacking sequence have similar behavior in energy harvesting system by changing frequency and electrical resistance. However, the output power amplitudes in each mode are significantly different for various composite plate case studies. For instant, the maximum output power at the first, second, third and fourth modes are related to case studies TC2, TC2, TC4, and TC1 with the values of 1.063, 9.028, 8.142 and 16.97 mW, respectively. The differences between the maximum and minimum output power among

Table 10 Comparison of maximum and minimum peak power outputs at each mode

Parameter	Maximum peak power output	Minimum peak power output	Difference (%)
First mode	1.063 mW-TC2	0.867 mW-TC4	22.6
Second mode	9.028 mW-TC2	5.482 mW-TC3	64.68
Third mode	8.142 mW-TC4	4.927 mW-TC1	65.25
Fourth mode	16.97 mW-TC1	9.579 mW-TC3	77.16

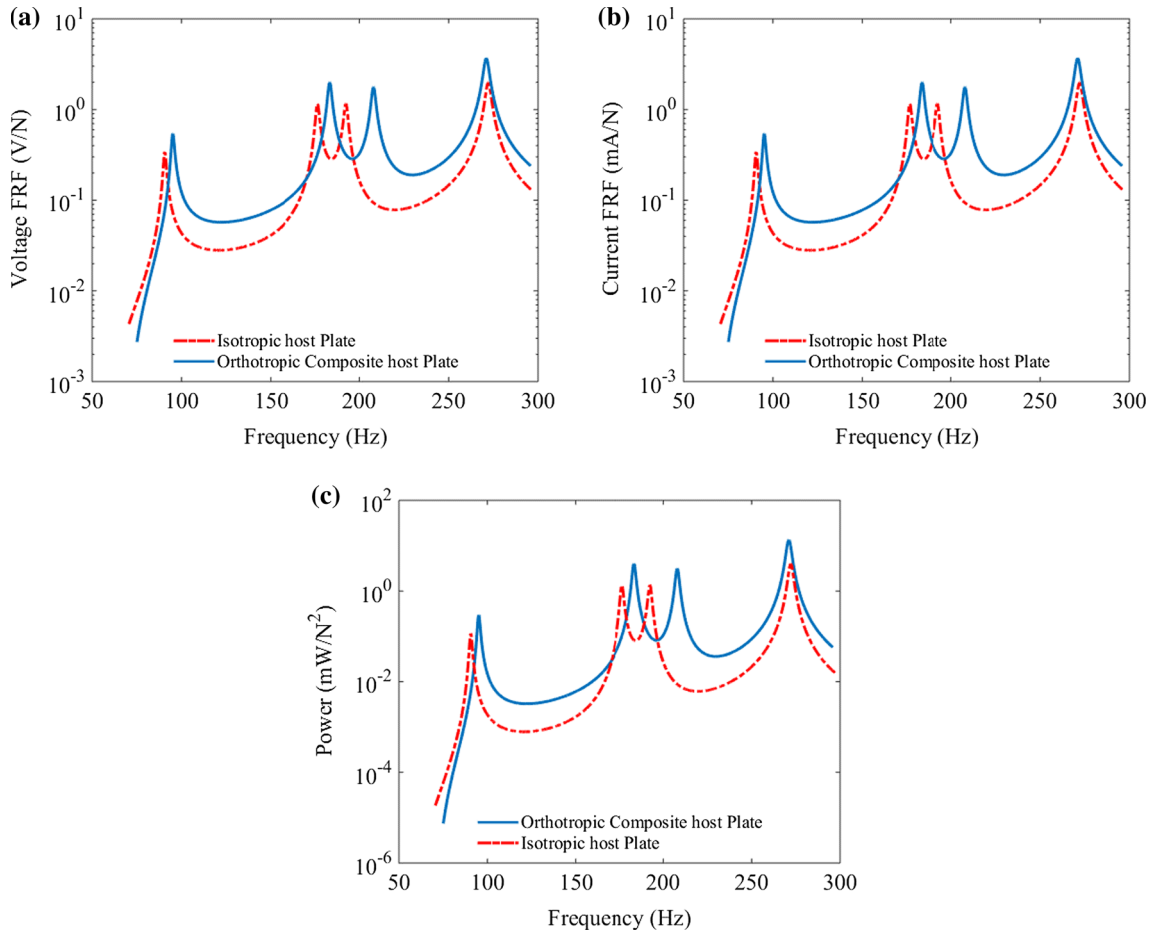

Fig. 12 Comparison of the isotropic and orthotropic plate's frequency responses for a load resistance of 1 kΩ: **a** voltage, **b** current, and **c** power

the all samples at each mode are shown in Table 10. Results show that the differences between maximum and minimum peak power output increase by raising natural frequency.

In order to study the effect of multilayered composite material of the host plate on the energy harvester's performance, the voltage, electric current and power FRFs of 1-layer isotropic aluminum and 8-layer carbon/epoxy orthotropic host plate TC1 are compared in Fig. 12. Both plates have the same geometry, boundary conditions and piezoelectric patch position based on Fig. 8, however, to prevent the emergence of anti-resonant frequency in isotropic host plate model, the excitation point force is located at (0.415, 0.155). It should be noted that the thickness of one-layer isotropic plate equals to total thickness of multilayer plate as $(h_s)_{iso} = (h_s)_{multilayer}$. In this example for isotropic plate, the aluminum material properties are considered as $E_1 = 70e9$ GPa, $\vartheta_{12} = 0.3$, $\rho = 2700$ kg/m^3, and also, the electrical resistance is assumed to be 1 kΩ, and also the natural frequencies as well as damping ratios are calculated and listed in Table 11.

Table 11 Natural frequencies and damping ratios of first four mode frequency for isotropic plate

Parameter	Mode 1 (1, 1)	Mode 2 (1, 2)	Mode 3 (2, 1)	Mode 4 (2, 2)
ζ	90.62/0.009	176.70/0.006	192.5/0.0061	272.2/0.0058

Table 12 Comparison of peak voltage outputs between isotropic and multilayer orthotropic host plate

Parameter	Orthotropic host plate	Isotropic host plate	Difference (%)
First mode	0.5425	0.3395	59.8
Second mode	2.0017	1.1570	73
Third mode	1.7725	1.160	52.8
Fourth mode	3.674	1.992	84.44

According to Fig. 12, the energy harvesting device with multilayer host plate behaves in a similar way with the isotropic one. Evaluating the results for first four resonances including 50–300 Hz shows that multilayer host plate leads to extracting higher output voltage, current as well as power from the energy harvester patch.

In order to compare results in more details, the peak values of voltage for either materials are tabulated at first four resonance frequencies in Table 12. According to the results, the generated output voltage from piezoceramic patch attached to multilayer orthotropic host structure are at least 52.8% more than the isotropic one despite 43.3% less mass.

4.3.2 Group B: effect of changing resistive load

In this section, changing resistive load on energy generated from piezoceramic patch attached on multilayer plate TC1 is analyzed in details as well. Frequency responses of electrical output parameters for a broad range of load resistance are investigated firstly, and then variation of peak amplitudes with changing the resistance load for the first four resonance frequencies are presented analytically.

4.3.2.1. *Frequency response for various load resistive*

The frequency responses of $[0/90/0/90]\,s$ composite plate TC1 including the output voltage, current as well as power are plotted in Fig. 13 for a wide range of electric resistance including 10–100 kΩ. It can be seen in Fig. 13a, b, with increasing the electric resistance from short circuit ($R \to 0$) to open-circuit ($R \to \infty$), the voltage increases and the electric current decreases among exciting frequencies, respectively. Therefore, for every excitation frequency, the maximum value of the voltage is obtained when the system is close to open-circuit conditions, and on the contrary to the voltage output, the maximum value of the electric current is extracted when the system is close to short-circuit condition. Furthermore, while increasing the resistance load, the resonance frequency of each vibration mode is moved a bit from the short-circuit resonance frequency to the open-circuit resonance frequency. In accordance with Fig. 13c, it is concluded that the results of output power do not necessarily display monotonic trend with increasing or decreasing the resistance load for a given frequency. Among the sample values of load resistance considered in present study, the maximum power output for the first vibration mode corresponds to the load of 10 kΩ at 95.1 Hz which is expectedly a frequency in between the fundamental short- and open-circuit resonance frequencies.

It is worth noting that the values of the load resistance used in this analysis are taken arbitrarily to observe the general trends. Therefore, the maximum power outputs obtained from each vibration mode are for these sample values and they are not necessarily for the maximum possible (or the optimized) power outputs.

4.3.2.2. *The peak amplitudes versus resistive load trends*

The variation of the output voltage, current as well as power with changing the resistance load for the first four resonance frequencies of $[0/90/0/90]\,s$ composite plate TC1 are plotted in Fig. 14. The results reveal that raising the resistive load in all vibration modes increases the voltage monotonically up to an asymptote which shows the maximum effective electric resistance. On the other hand, the generated electric current shows an opposite behavior, which means that increasing the electric resistance has no effect up to a specified value. Indeed, the output current is very insensitive when the system is close to short-circuit conditions and then, starts decreasing for the open-circuit resonance frequency. Figure 14c shows the trend of electrical power generated

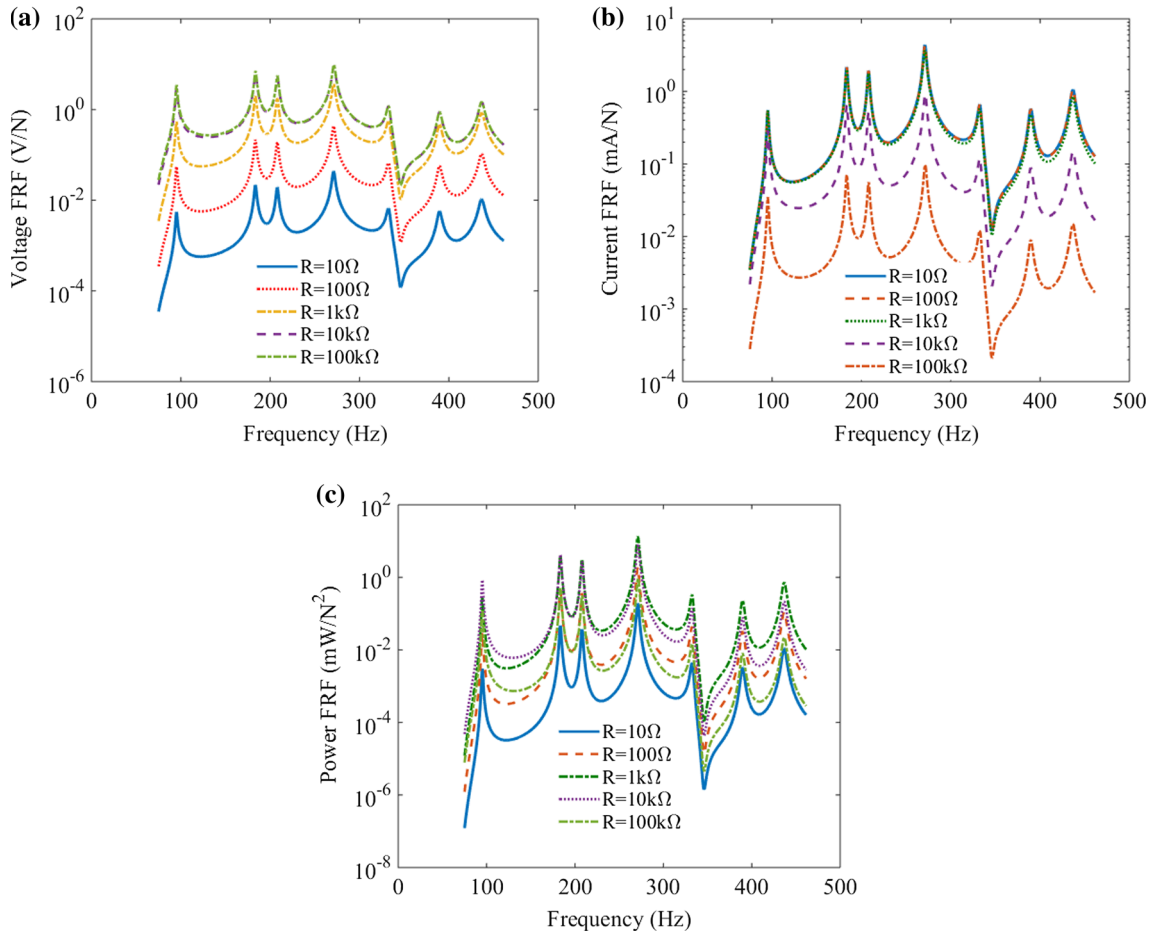

Fig. 13 Electric resistance load effects on **a** voltage; **b** current and **c** power FRFs

by the piezoelectric patch with changing resistive load at the first four resonance frequencies. The power curves have similar trends for each vibration mode, but it does not exhibit a monotonic behavior with changing the load resistance. Hence, the variation of output power with changing the electric resistance exhibits an optimum resistive load which leads to a maximum peak output power. Furthermore, as it is expected, the maximum value of electric power occurs at the forth mode.

5 Conclusion

Multilayer orthotropic composite plates with different boundary conditions are applicable in several engineering systems. Therefore, integrated piezoelectric patch-based energy harvester in the neighborhood of these structures compared to single-layer isotropic one will lead to producing more efficient self-powered energy harvesting systems using mechanical vibration. In this study, an analytical electroelastic model of piezoelectric energy harvester patch structurally integrated to a thin multilayer orthotropic host plate was developed based on distributed parameter modeling approach. For the special case of transversely applied point force excitation, the closed-form steady-state expressions were formulated for the electromechanically coupled vibration and electrical response. Comparing the results of the voltage FRF as well as peak voltage vs resistance given by analytical solution with numerical method proved the analytical formulation validity to calculate the generated voltage. To this end, three-dimensional finite-element (FE) analysis was conducted using the commercial software ANSYS. After verifying the formulations, it was needed to specify parameters in energy harvesting model, so, the positioning of the piezoceramic patch and point force excitation was discussed for voltage generation from multiple vibration modes model based on the mode shape dependent dynamic strain distribution. Then, the effects of various stacking sequences of the host plate on piezoelectric energy harvesting are presented

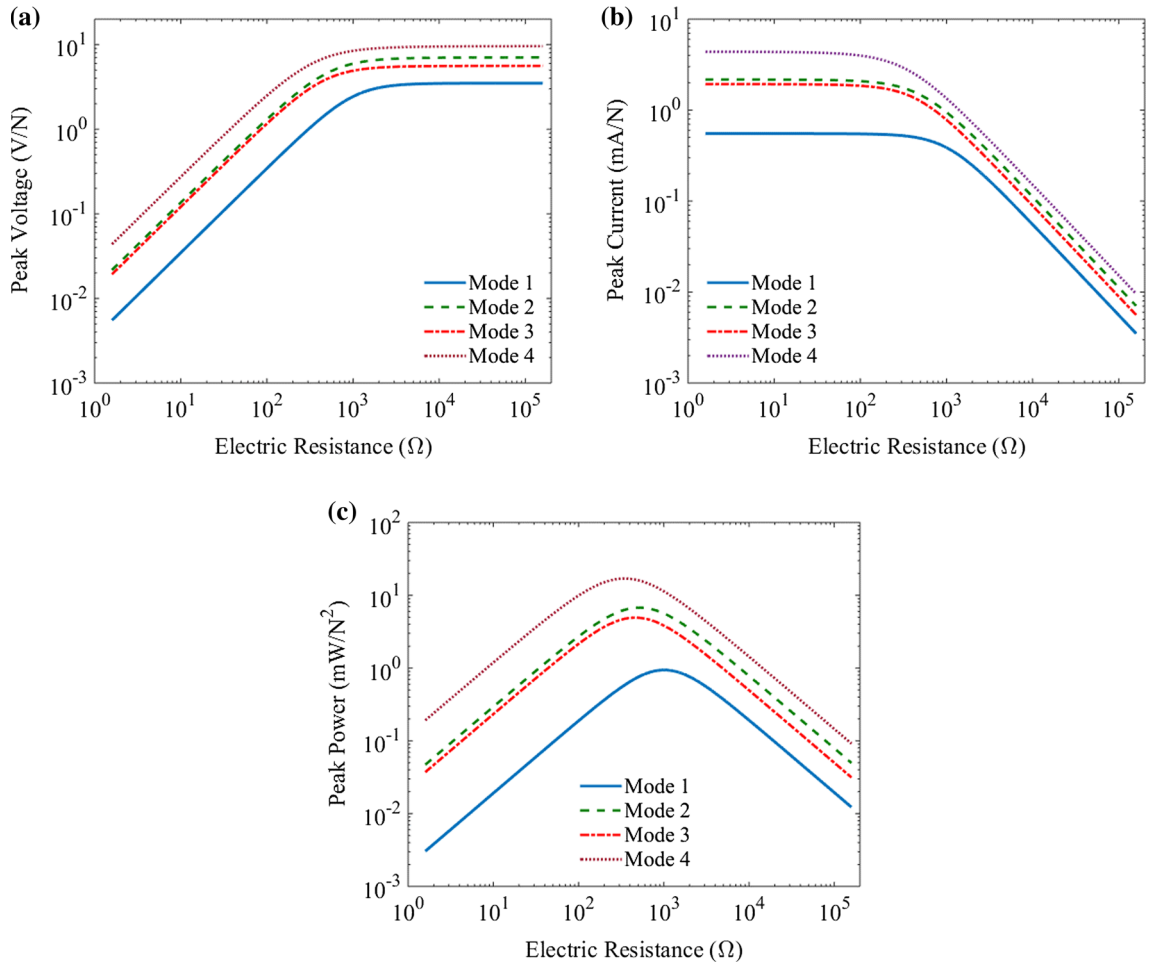

Fig. 14 Variation of the **a** peak voltage; **b** peak current; **c** peak power output with load resistance at resonance frequencies of the first four modes

through the parametric study. Also, the obtained result has indicated that vibration of multilayer orthotropic host plate generated more voltage output from piezoelectric patch harvester than single-layer isotropic one, despite less mass density. The analytical FRFs response including voltage, current as well as power output were discussed for a broad range of load resistance. Then, the results of peak voltage, current as well as power output are plotted against the load resistance to exhibit an optimum resistive load. It has been noted that, the electroelastic FRFs framework corresponding to the voltage, current, power outputs and vibration response to force input can be utilized for each multilayer and single-layer host plate with different material properties including orthotropic or isotropic. Consequently, the electroelastic model developed herein can be used for design, performance optimization and optimal positioning of the harvester patch and force excitation on the host structure for multi-mode energy harvesting.

References

1. Roundy, S., Wright, P.K., Rabaey, J.: A study of low level vibrations as a power source for wireless sensor nodes. Comput. Commun. **26**, 1131–1144 (2003)
2. Zhu, P., Ren, X., Qin, W., Zhou, Z.: Improving energy harvesting in a tri-stable piezomagnetoelastic beam with two attractive external magnets subjected to random excitation. Arch. Appl. Mech. **87**(1), 45–57 (2017)
3. Gao, Y.H., Jiang, S.N., Zhu, D.B., Gao, H.T.: Theoretical analysis of a piezoelectric ceramic tube polarized tangentially for hydraulic vibration energy harvesting. Arch. Appl. Mech. **87**(4), 607–615 (2017)
4. Anton, S.R., Sodano, H.A.: A review of power harvesting using piezoelectric materials (2003–2006). Smart Mater. Struct. **16**, R1–R21 (2007)

5. Xie, X.D., Wang, Q., Wu, N.: Energy harvesting from transverse ocean waves by a piezoelectric plate. Int. J. Eng. Sci. **81**, 41–48 (2014)
6. Akbar, M., Curiel-Sosa, J.L.: Piezoelectric energy harvester composite under dynamic bending with implementation to aircraft wingbox structure. Compos. Struct. **153**, 193–203 (2016)
7. Xie, X.D., Wu, N., Yuen, K.V., Wang, Q.: Energy harvesting from high-rise buildings by a piezoelectric coupled cantilever with a proof mass. Int. J. Eng. Sci. **72**, 98–106 (2013)
8. Paradiso, J.A., Starner, T.: Energy scavenging for mobile and wireless electronics. IEEE Pervasive Comput. **4**, 18–27 (2005)
9. Naruse, Y., et al.: Electrostatic micro power generation from low-frequency vibration such as human motion. J. Micromech. Microeng. **19**, 094002 (2009)
10. Chiu, Y., Tseng, V.F.G.: A capacitive vibration to electricity energy converter with integrated mechanical switches. J. Micromech. Microeng. **18**, 104004 (2008)
11. Lee, C., et al.: Theoretical comparison of the energy harvesting capability among various electrostatic mechanisms from structure aspect. Sens. Actuators A **156**, 208–216 (2009)
12. Beeby, S.P., et al.: A micro electromagnetic generator for vibration energy harvesting. J. Micromech. Microeng. **17**, 1257–1265 (2007)
13. Yang, B., et al.: Electromagnetic energy harvesting from vibrations of multiple frequencies. J. Micromech. Microeng. **19**, 035001 (2009)
14. Wang, L., Yuan, F.G.: Vibration energy harvesting by magnetostrictive material. Smart Mater. Struct. **17**, 045009 (2008)
15. Adly, A., et al.: Experimental tests of a magnetostrictive energy harvesting device toward its modeling. J. Appl. Phys. **107**, 09A935 (2010)
16. Tiwari, R., Kim, K.J., Kim, S.M.: Ionic polymer-metal composite as energy harvesters. Smart Struct. Syst. **4**(5), 549–563 (2008)
17. Yiming, L., et al.: Investigation of electrostrictive polymers for energy harvesting. IEEE Trans. Ultrason. Ferroelectr. Freq. Control **52**, 2411–2417 (2005)
18. Wang, Z.L., Song, J.: Piezoelectric nanogenerators based on zinc oxide nanowire arrays. Science **312**, 242–246 (2006)
19. Cook-Chennault, K.A., Thambi, N., Sastry, A.M.: Powering MEMS portable devices—a review of non-regenerative and regenerative power supply systems with special emphasis on piezoelectric energy harvesting systems. Smart Mater. Struct. **17**, 043001 (2008)
20. Erturk, A., Inman, D.J.: A distributed parameter electromechanical model for cantilevered piezoelectric energy harvesters. J. Vib. Acoust. **130**, 041002 (2008)
21. Erturk, A., Inman, D.J.: Piezoelectric Energy Harvesting. Wiley, Hoboken (2011)
22. Erturk, A.: Assumed modes modeling of piezoelectric energy harvesters: Euler–Bernoulli, Rayleigh, and Timoshenko models with axial deformations. Comput. Struct. **106**(107), 214–227 (2012)
23. Amini, Y., Emdad, H., Farid, M.: Finite element modeling of functionally graded piezoelectric harvesters. Compos. Struct. **129**, 165–176 (2015)
24. Amini, Y., Fatehi, P., Heshmati, M., Parandvar, H.: Time domain and frequency domain analysis of functionally graded piezoelectric harvesters subjected to random vibration: finite element modeling. Compos. Struct. **136**, 384–393 (2016)
25. Dai, H.L., Wang, Y.K., Wang, L.: Nonlinear dynamics of cantilevered microbeams based on modified couple stress theory. Int. J. Eng. Sci. **94**, 103–112 (2015)
26. Erturk, A., Inman, D.J.: An experimentally validated bimorph cantilever model for piezoelectric energy harvesting from base excitations. Smart Mater. Struct. **18**, 025009 (2009)
27. Zhao, S., Erturk, A.: Electroelastic modeling and experimental validations of piezoelectric energy harvesting from broadband random vibrations of cantilevered bimorphs. Smart Mater. Struct. **22**, 015002 (2013)
28. Dietl, J.M., Wickenheiser, A.M., Garcia, E.: A Timoshenko beam model for cantilevered piezoelectric energy harvesters. Smart Mater. Struct. **19**, 055018 (2010)
29. Yang, Y., Tang, L.: Equivalent circuit modeling of piezoelectric energy harvesters. J. Intell. Mater. Syst. Struct. **20**, 2223–2235 (2009)
30. Cottone, F., et al.: Piezoelectric buckled beams for random vibration energy harvesting. Smart Mater. Struct. **21**, 035021 (2012)
31. Friswell, M.I., et al.: Nonlinear piezoelectric vibration energy harvesting from a vertical cantilever beam with tip mass. J. Intell. Mater. Syst. Struct. **23**, 1505–1521 (2012)
32. Friswell, M.I., Adhikari, S.: Sensor shape design for piezoelectric cantilever beams to harvest vibration energy. J. Appl. Phys. **108**, 014901 (2010)
33. Lallart, M., Guyomar, D.: Piezoelectric conversion and energy harvesting enhancement by initial energy injection. Appl. Phys. Lett. **97**, 014104 (2010)
34. Erturk, A., Inman, D.J.: Issues in mathematical modeling of piezoelectric energy harvesters. Smart Mater. Struct. **17**, 065016 (2008b)
35. Shahruz, S.M.: Design of mechanical band-pass filters with large frequency bands for energy scavenging. Mechatronics **16**, 523–531 (2006)
36. Song, H.J., Choi, Y.-T., Purekar, A.S., et al.: Performance evaluation of multi-tier energy harvesters using macrofiber composite patches. J. Intell. Mater. Syst. Struct. **20**, 2077–2088 (2009)
37. Erturk, A., Renno, J.M., Inman, D.J.: Modeling of piezoelectric energy harvesting from an L-shaped beammass structure with an application to UAVs. J. Intell. Mater. Syst. Struct. **20**, 529–544 (2009b)
38. Friswell, M.I., Adhikari, S.: Sensor shape design for piezoelectric cantilever beams to harvest vibration energy. J. Appl. Phys. **108**, 014901–014906 (2010)
39. Huan, X., Yuantai, H., Qing-Ming, W.: Broadband piezoelectric energy harvesting devices using multiple bimorphs with different operating frequencies. IEEE Trans. Ultrason. Ferroelectr. Freq. Control **55**, 2104–2108 (2008)
40. Lien, I.C., Shu, Y.C.: Array of piezoelectric energy harvesting by the equivalent impedance approach. Smart Mater. Struct. **21**, 082001 (2012)

41. Huang, S.-C., Lin, K.-A.: A novel design of a maptuning piezoelectric vibration energy harvester. Smart Mater. Struct. **21**, 085014 (2012)
42. Salmani, H., Rahimi, G.H., Hosseini Kordkheili, S.A.: An exact analytical solution to exponentially tapered piezoelectric energy harvester. Shock Vib. (2015). https://doi.org/10.1155/2015/426876
43. Paknejad, A., Rahimi, G.H., Farrokhabadi, A., Khatibi, M.M.: Analytical solution of piezoelectric energy harvester patch for various thin multilayer composite beams. Compos. Struct. **154**, 694–706 (2016)
44. Bayik, B., Aghakhani, A., Basdogan, I., Erturk, A.: Equivalent circuit modeling of a piezo-patch energy harvester on a thin plate with AC–DC conversion. Smart Mater. Struct. **25**(5), 055015 (2016)
45. Aridogan, U., Basdogan, I., Erturk, A.: Analytical modeling and experimental validation of a structurally integrated piezoelectric energy harvester on a thin plate. Smart Mater. Struct. **23**, 045039 (2014)
46. Aridogan, U., Basdogan, I., Erturk, A.: Random vibration energy harvesting on thin plates using multiple piezopatches. J. Intell. Mater. Syst. Struct. (2016). https://doi.org/10.1177/1045389X16635846
47. Erturk, A.: Piezoelectric energy harvesting for civil infrastructure system applications: moving loads and surface strain fluctuations. J. Intell. Mater. Syst. Struct. **22**, 1959–1973 (2011)
48. Aridogan, U., Basdogan, I., Erturk, A.: Multiple patch-based broadband piezoelectric energy harvesting on plate-based structures. J. Intell. Mater. Syst. Struct. **25**, 1664–1680 (2014)
49. De Marqui, C., Erturk, A., Inman, D.J.: Piezoaeroelastic modeling and analysis of a generator wing with continuous and segmented electrodes. J. Intell. Mater. Syst. Struct. **21**, 983–993 (2010)
50. De Marqui, C., et al.: Modeling and analysis of piezoelectric energy harvesting from aeroelastic vibrations using the doublet-lattice method. J. Vib. Acoust. Trans. ASME **133**, 011003 (2011)
51. Rupp, C.J., et al.: Design of piezoelectric energy harvesting systems: a topology optimization approach based on multilayer plates and shells. J. Intell. Mater. Syst. Struct. **20**, 1923–1939 (2009)
52. Jones, R.M.: Mechanics of Composite Materials. Taylor & Frances Inc, Oxford (1999)
53. Gibson, R.F.: A review of recent research on mechanics of multifunctional composite materials and structures. Compos. Struct. **92**(12), 2793–2810 (2010)
54. Pellegrini Sergio, P., et al.: Bistable vibration energy harvesters: a review. J. Intell. Mater. Syst. Struct. **24**(11), 1303–1312 (2012)
55. Harne, R.L., Wang, K.W.: A review of the recent research on vibration energy harvesting via bistable systems. J. Smart Mater. Struct. **2013**(22), 023001 (2013)
56. Brampton Christopher, J., et al.: Sensitivity of bistable laminates to uncertainties in material properties, geometry and environmental conditions. J. Compos. Struct. **102**, 276–286 (2013)
57. Jong-Gu, L., et al.: Effect of initial tool-plate curvature on snap-through load of unsymmetric laminated cross-ply bistable composites. J. Compos. Struct. **122**, 82–91 (2015)
58. Mehdi, Tavakkoli S., et al.: An analytical study on piezoelectric-bistable laminates with arbitrary shapes for energy harvesting. In: 7th ECCOMAS Thematic Conference on Smart Structures and Materials (2015)
59. Arrieta, A.F., et al.: A piezoelectric bistable plate for nonlinear broadband energy harvesting. J. Appl. Phys. Lett. **97**, 104102 (2010)
60. Betts, D.N., et al.: Optimal configurations of bistable piezo-composites for energy harvesting. J. Appl. Phys. Lett. **100**(11), 114104 (2012)
61. Betts, D.N., et al.: Preliminary study of optimum piezoelectric cross-ply composites for energy harvesting. J. Smart Mater. Res. (2012). https://doi.org/10.1155/2012/621364
62. Syta, A., Bowen, C.R., Kim, H.A., Rysak, A., Litak, G.: Experimental analysis of the dynamical response of energy harvesting devices based on bistable laminated plates. Meccanica **50**(8), 1961–1970 (2015)
63. Betts, D.N., Bowen, C.R., Kim, H.A., Gathercole, N., Clarke, C.T., Inman, D.J.: Nonlinear dynamics of a bistable piezoelectric-composite energy harvester for broadband application. Eur. Phys. J. Spec. Top. **222**(7), 1553–1562 (2013)
64. Xing, Y.F., Liu, B.: New exact solutions for free vibrations of thin orthotropic rectangular plates. Compos. Struct. **89**, 567–574 (2009)
65. Her, S.-C., Lin, C.-S.: Vibration analysis of composite laminate plate excited by piezoelectric actuators. Sensors **13**(3), 2997–3013 (2013)